FULL PAPER

Magnetic Resonance in Medicine 00:00–00 (2014)

Real-Time Correction of Rigid Body Motion-Induced Phase Errors for Diffusion-Weighted Steady-State Free Precession Imaging

Rafael O'Halloran,* Murat Aksoy, Eric Aboussouan, Eric Peterson, Anh Van, and Roland Bammer

Purpose: Diffusion contrast in diffusion-weighted steady-state free precession magnetic resonance imaging (MRI) is generated through the constructive addition of signal from many coherence pathways. Motion-induced phase causes destructive interference which results in loss of signal magnitude and diffusion contrast. In this work, a three-dimensional (3D) navigator-based real-time correction of the rigid body motion-induced phase errors is developed for diffusion-weighted steady-state free precession MRI.

Methods: The efficacy of the real-time prospective correction method in preserving phase coherence of the steady state is tested in 3D phantom experiments and 3D scans of healthy human subjects.

Results: In nearly all experiments, the signal magnitude in images obtained with proposed prospective correction was higher than the signal magnitude in images obtained with no correction. In the human subjects, the mean magnitude signal in the data was up to 30% higher with prospective motion correction than without. Prospective correction never resulted in a decrease in mean signal magnitude in either the data or in the images.

Conclusions: The proposed prospective motion correction method is shown to preserve the phase coherence of the steady state in diffusion-weighted steady-state free precession MRI, thus mitigating signal magnitude losses that would confound the desired diffusion contrast. **Magn Reson Med 000:000–000, 2014. © 2014 Wiley Periodicals, Inc.**

Key words: diffusion; steady-state free precession; phase; diffusion-weighted imaging (DWI); motion-correction; navigation; diffusion tensor imaging (DTI)

INTRODUCTION

In a majority of clinical magnetic resonance imaging (MRI) sequences, multishot imaging is used to achieve high spatial resolution without incurring off-resonance artifacts associated with long readouts. Diffusion-weighted MRI, however, is still limited to sequences based on single-shot echo-planar imaging (EPI) due to the problem of motion-induced phase inconsistencies between shots. This problem has been previously addressed by the use of navigator echoes (1–3) and later by the use of self-navigated sequences such as PROPELLER and short-axis propeller EPI (SAP-EPI) (4). However, at high-resolution, these approaches are associated with increased scan time and limited efficiency.

Diffusion-weighted steady-state free precession (DW-SSFP) imaging is a technique recently investigated (5–8) as a way to address the resolution limitations of diffusion-weighted MRI. DW-SSFP is efficient since the ratio of readout time to diffusion-weighting time can be higher than that of spin echo diffusion. However, in DW-SSFP, a constant 90-degree phase between the radiofrequency (RF) pulse and transverse magnetization is required for the maintenance of the steady state. Motion corrupts this relationship by introducing additional phase to the transverse magnetization and leads, therefore, to loss of signal magnitude and diffusion contrast. Retrospective phase correction can be used to mitigate some of these errors; however, the reduction in the steady-state signal magnitude is irrecoverable (8). To fully correct these errors, a prospective phase correction (ProCo) technique is required.

To date, no ProCo has been presented for DW-SSFP; however, ProCo has been demonstrated to be effective in two-dimensional (2D) multishot diffusion-weighted techniques such as RARE (9) and FLASH (10). In these correction techniques, rigid body (RB) motion-induced phase errors were corrected by applying gradient pulses to cancel linear phase terms and by applying a pulse to the B_0 field to cancel the constant phase term. Recently, Nunes et al. (11) presented an RF-based correction for non-RB motion-induced phase errors in fast spin echo (FSE).

A similar approach can be used for DW-SSFP. DW-SSFP is an attractive candidate for navigated multishot diffusion, as its diffusion-encoding gradients are relatively short, leading to less induced phase for a given amount of motion. This means the navigator requires a lower k-space coverage compared to conventional Stejskal–Tanner diffusion preparations to achieve the same motion sensitivity. This work is focused on the development and demonstration of a technique for the prospective correction of RB motion-induced phase (ProCo) for use in a 3D DW-SSFP sequence. The central hypothesis

Department of Radiology, Stanford University, Stanford, California, USA

Grant sponsor: NIH; Grant numbers: 1 R01 EB008706; 1 R01 EB008706 S1; 5 R01 EB002711; 1 R01 EB006526; 1 R21 EB006860; Grant sponsor: Center of Advanced MR Technology at Stanford; Grant number: P41RR09784; Grant sponsor: Lucas Foundation, Oak Foundation and GE Healthcare.

*Correspondence to: Rafael O'Halloran, Ph.D., Room 1–115, Hess Center, Icahn School of Medicine at Mount Sinai. 1470 Madison Ave, New York, NY 10128. E-mail: rafael.o'halloran@mssm.edu

Received 16 September 2013; revised 8 January 2014; accepted 10 January 2014

DOI 10.1002/mrm.25159

Published online 00 Month 2014 in Wiley Online Library (wileyonlinelibrary.com).

Table 1
A Summary of the Effects of RB, in Images Space (column 2), k-Space (column 3), and the Way to Correct them in the Pulse Sequence (column 4)

Type of motion	Effect in image space	Effect in k-space	Hardware correction
Translation	Constant phase	Constant phase	Phase of applied RF
Rotation	Linear phase	Shift of k-space center	Blip gradients

Note that, for simplicity this table assumes rotation on isocenter. For rotation off isocenter, a constant phase component will also be induced and will therefore be corrected by the RF pulse along with translational motion.

of the work is that the use of ProCo will result in higher steady-state magnitude signal compared to a scan without the use of ProCo and that these increases in steady-state magnitude signal will result in analogous increases in the magnitude of the signal in resulting images. The efficacy of ProCo in preserving the steady-state signal magnitude and in increasing the signal magnitude in reconstructed images will be demonstrated in phantom experiments and in healthy human subjects.

THEORY

Motion and Phase

The purpose of this work is to address the issue of RB phase in DW-SSFP imaging of the brain. The justification for limiting this method to RB motion is based on a model of brain motion in which RB and non-RB motion are treated separately (12). In this model, the RB component accounts for the majority of total motion and arises from unpredictable motion of the head, vibration, and some repeatable sources such as breathing and cardiac motion. The non-RB component is lower in magnitude, highly correlated with the cardiac cycle, and predictable. The RB component, therefore, is the most important component to be measured at each pulse repetition time (TR).

The transverse magnetization of an object moving in a magnetic field gradient will accrue a phase (13). The phase profile across the object (in image space) will depend on the type of motion the object undergoes. For the special case of RB motion, a combination of translation and rotation, this phase has simple spatial dependence. The translational component of the motion along the diffusion-encoding gradient results in a constant phase, whereas rotational components with axes of rotations perpendicular to the diffusion-encoding gradient result in linearly varying phase perpendicular to the axis of rotation. To understand the implication of this phaseon navigation, it is helpful to visualize the effect in k-space. The constant image space phase induced by translation looks the same in k-space, as the constant phase term, being spatially invariant, can be written outside of the Fourier integral. The linear image space phase induced by rotation causes a shift in k-space according to the Fourier shift theorem. Table 1 summarizes these effects.

The Effect of Motion on the Steady State

For a DW-SSFP sequence in the steady state, the phase of the transverse magnetization is 90 degrees from the phase of the RF pulse at the time when the RF pulse is played out. Motion during the diffusion-encoding gradients induces an additional phase on the transverse magnetization, such that the coherence pathways generated by the next RF pulse, are distributed differently from the steady state, thus disrupting the steady state. This disruption ultimately leads to loss of signal and contrast during the transient period required to recover the steady state. In the case of continuous bulk motion or flow, the constant introduction of quasirandom phase leads to a condition akin to RF spoiling (14), in which the added phase due to motion maintains the magnetization in a transient state, preventing it from reaching steady state. The propagation of phase errors accrued in a given TR to subsequent TR's and subsequent signal loss is the reason why ProCo is needed in steady-state sequences. Note that, this motion-induced signal loss relative to the "unweighted" diffusion scan leads to an overestimation of the diffusion coefficient. In nonsteady-state sequences, such as a navigated multishot EPI, the magnitude of the signal is unaffected by motion and it, therefore, suffices to measure the phase with a navigator and correct it retrospectively.

Because the disruption of the steady state is caused by the disruption of the 90-degree phase relationship between the RF pulse and transverse magnetization at the time the RF pulse is played out, it can be corrected prospectively by measuring the transverse phase and ensuring that the relationship holds over the imaging volume. In general, the motion-induced transverse phase has arbitrary spatial dependence but in this work, the scope is limited to the RB motion-induced components, that is, the constant and linear terms. The constant terms can be corrected by matching the phase of the RF pulse to the phase of the transverse magnetization. Conversely, one could unwind the constant phase term by applying a pulse to the B_0 coil as in Norris and Driesel (9); however, rapid control of B_0 is not available on most commercial MRI systems. The linear term can be unwound by the use of magnetic field gradient pulses on each axis (9).

Why Retrospective Phase Correction is Needed in Addition to Proco

The purpose of ProCo is to prevent motion-induced phase errors accrued in a given TR from propagating into future TRs and disrupting the steady state. Even if ProCo works perfectly, retrospective correction is needed to correct the phase disparities between shots. A look at the timing of the pulse sequence is helpful in understanding this issue (Fig. 1). In a given TR, the motion is measured with the navigator and processed during the readout of the imaging interleaf for that TR (Fig. 1c). The adaptive

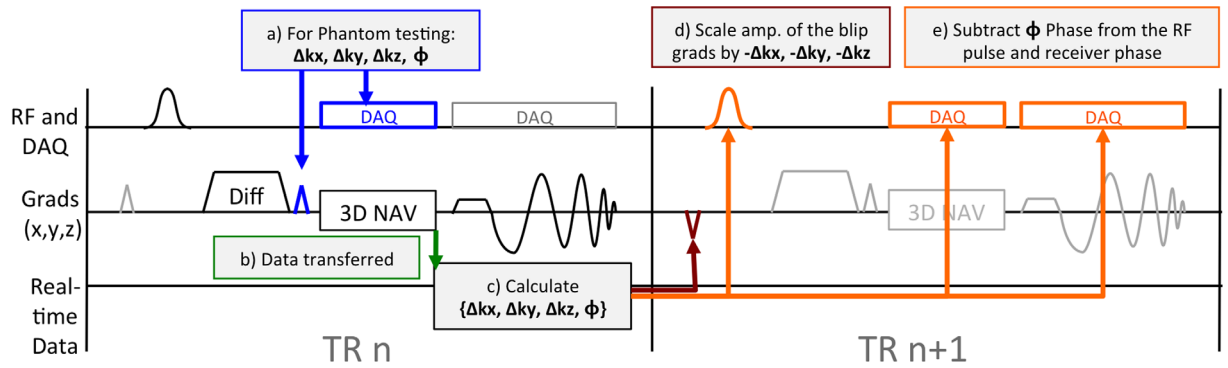

FIG. 1. A schematic of the pulse sequence with two consecutive TRs to show how navigator data acquired in TR *n* is used to correct the motion-induced phase by applying a correction in TR $n+1$. The navigator data are acquired and transferred to the motion correction system (**b**). The motion parameters are computed, while the imaging readout is acquired (**c**). In TR $n+1$, the parameters computed during TR *n* are used to correct the RB motion-induced phase by setting the amplitudes of the correction blips (**d**), and the phase of the RF excitation pulse (**e**). The receivers are also modulated by the same phase as the RF pulse for convenience in reconstruction (e). Optional blip gradients and data acquisition window modulation are available for testing in phantoms (a). [Color figure can be viewed in the online issue, which is available at wileyonlinelibrary.com.]

correction of the measured phase is applied via RF phase and correction blip gradients during the next TR, so the acquired imaging interleaf will be uncorrected; it will be modulated by the motion-induced phase arising from that TR. The retrospective correction removes this phase during the reconstruction using the same navigator echo used in ProCo. Note that, the requirement of the retrospective correction could be eliminated in principle if the real-time processing of ProCo were so fast that the corrections could be applied before the imaging readout. However, due to practical considerations on our system, this is not currently possible without introducing a large delay before the imaging readout.

Measurement of the Motion

The motion-induced phase can be measured from a navigator image, $I(\mathbf{r},t)$, with the form

$$I(\mathbf{r},t) = m(\mathbf{r})e^{i\Phi(\mathbf{r},t)}, \quad [1]$$

where $m(\mathbf{r})$ is the magnitude of the image, t is the number of the TR, and $\mathbf{r}$ is the position in space. Note that, since navigator images are collected once per TR, t is discretized in multiples of TR. Some of the phase, $\Phi(\mathbf{r},t)$, arises from motion, whereas the rest arises from other sources such as eddy currents and coil sensitivities (12). To isolate the component due to motion, the navigator images, $I(\mathbf{r},t)$, can be compared to a motion-free reference image,

$$I_{\text{ref}}(\mathbf{r}) = m_{\text{ref}}(\mathbf{r})e^{i\Phi_{\text{ref}}(\mathbf{r})}, \quad [2]$$

The reference image will be discussed in more detail in the next section. With this motion-free reference image, the motion-induced phase, $\Phi_m(\mathbf{r},t)$ can be isolated:

$$\Phi_m(\mathbf{r},t) = \Phi(\mathbf{r},t) - \Phi_{\text{ref}}(\mathbf{r}). \quad [3]$$

In general, the phase due to motion has arbitrary spatial dependence, but as this work is limited to the RB motion-induced components, that is the zero- and first-order terms, the phase is expanded and truncated at the second term,

$$\Phi_m(\mathbf{r},t) = \sum_{n=0}^{\infty} \mathbf{a_n}(t)\cdot\mathbf{r}^n \approx a_0(t) + \mathbf{a_1}(t)\cdot\mathbf{r}. \quad [4]$$

So the problem of measuring the RB motion-induced phase is to determine the scalar coefficient a_0 and the vector $\mathbf{a_1}$ for each TR, t. The three components of the linear term, $\mathbf{a_1}$, can be found easily (15) by multiplying the navigator image, $I(\mathbf{r})$, by the conjugate of the same image shifted by one pixel along each principle direction, and taking the phase of that product. For example, the x-component of $\mathbf{a_1}$ is obtained by:

$$\mathbf{a_1}\cdot\hat{\imath} = -\arg\left(I(\mathbf{r})I^*(\mathbf{r}+\hat{\imath})I^*_{\text{ref}}(\mathbf{r})I_{\text{ref}}(\mathbf{r}+\hat{\imath})\right), \quad [5]$$

where $\hat{\imath}$ is the unit vector along x and the explicit dependence on t is dropped for clarity. Note that this result can be obtained on each pixel and averaged to get a better estimate of $\mathbf{a_1}$. Also note that, for each term in I there is a conjugate term in I_{ref} to satisfy the subtraction relationship in Eq. [3]. In Ahn and Cho (15), a histogram analysis was used to obtain a_0; however, because the present work is concerned with fast prospective correction, a simpler approach is taken. Once the $\mathbf{a_1}$ has been determined by Eq. [5], the contribution to the phase of the reference image of the linear term can be removed to estimate the a_0 term:

$$a_0 = \arg\left(I(\mathbf{r})I^*_{\text{ref}}(\mathbf{r})e^{-i\mathbf{a_1}\cdot\mathbf{r}}\right). \quad [6]$$

Again the a_0 term can be computed for each pixel and then averaged to obtain a better estimate. In practice, averaging is done by complex summation over $\mathbf{r}$ inside the arg function.

The Reference Navigator Image

The reference navigator image is used to remove any image phase arising from sources other than motion from

the calculation of the motion parameters, a_0 and $\mathbf{a_1}$. Although some retrospective techniques obtain the reference navigator image from the unweighted scan, this is not desirable in a prospectively corrected sequence due to the eddy current-induced phase term, (12) which are different in the unweighted image and the diffusion-weighted images. Because eddy currents in the diffusion-weighted image differ from those in the unweighted image, it will always appear to the motion correction system that motion is occurring if the unweighted navigator is used as a reference phase. Furthermore, contributions due to imaging gradients will also appear to the motion correction system to be motion. These sources of phase that appear to be motion will cause the ProCo system to add unwanted phase. Note that, in retrospective corrections, this is not a problem because the correction of one interleaf of data (i.e., collected in a single TR or shot) will not effect subsequent interleaves as it does in prospective systems.

To include this eddy current term in the reference navigator image, it is necessary to obtain the reference navigator image from the diffusion-weighted image series itself. However, this presents a problem: as the diffusion-weighted images are sensitive to motion-induced phase, it is impossible to know which navigator images are free of motion-induced phase. To deal with this issue, the reference image can be obtained via a sliding window averaging approach, assuming that over the time scale of the sliding window, the motion-induced phase sums to zero. The reference navigator image is then,

$$I_{\text{ref}}(\mathbf{r}, t) = \sum_{\tau=0}^{t-1} f^{t-\tau} I(\mathbf{r}, \tau) \qquad [7]$$

where f is a number between 0 and 1 that adjusts the contribution of past navigator images to the reference for a given TR, t. Thus, navigators further back in time contribute less to the reference image than more recently acquired ones. With an appropriate choice of f, this method provides a stable reference, free of confounding motion-induced phase, that allows for slow drift such as B_0 drift and drifts in eddy currents due to imaging gradient cycling. In human imaging for instance, a suitable choice of f would allow accrual of reference data over a time scale comparable to a few heartbeats since the motion-induced phase is known to be periodic with heartbeat (12). If the TR is 25 ms for example, and the heart rate is 1 Hz, then an f of 0.99 would mean that a navigator image from six cardiac cycles ago would contribute about 9% of its signal to the reference phase image. For imaging in phantoms in which no such periodicity exists, the choice is somewhat arbitrary as any motion induced is artificial.

METHODS

Simulations

The physics of the DW-SSFP sequence was simulated with extended phase graphs with an additional module to simulate motion. Motion during the diffusion-encoding gradient was simulated by adding a phase to the transverse dephasing states immediately after the diffusion-encoding gradient. To demonstrate the effect of motion on the signal in a single pixel, the time course of a pixel was simulated over 200 TRs with three types of motion: an impulsive motion occurring during a single TR, random motion during every TR, and pulsatile motion. The impulsive motion was such that it imparted 180 degrees of phase to the transverse magnetization. The random motion produced phase that was zero-mean, Gaussian-distributed with a standard deviation of 60 degrees. The pulsatile motion was a simulated cardiac-like waveform that had periodic triangular spikes separated by longer periods of slower opposite motion with a maximum and minimum of 150 and 46, degrees respectively.

To investigate the effects of motion over a wider range of motions and flip angles, the impulsive motion experiment was repeated with motion-induced phases ranging from 0 to 360 degrees and for flip angles of 10, 20, 30, 40, and 50degrees. The loss in signal was assessed by computing the integral of the difference between the steady-state signal curves with and without motion. The integrals were normalized by the steady-state signal magnitude to obtain the relative signal loss in units of a percentage times the number of TRs. Thus, a relative signal loss of 100 could mean complete signal loss for 1 TR or 1% loss for 100 TRs. It is a metric for the total impact of motion during a single TR on subsequent TRs.

Magnetic Resonance Imaging

Imaging was performed on a 3T scanner with a eight-channel receive-only head coil (GE Healthcare, Waukesha, WI) using a navigated 3D DW-SSFP sequence (8) consisting of a water-selective RF pulse, trapezoidal diffusion-encoding gradient with a 6-ms plateau and 1-ms ramps, 3D navigator, then a spiral projection readout interleaf (16). An overview of the sequence is given in Figure 1; two successive TRs are shown in the context of the proposed ProCo system. Imaging parameters were: TR = 34 ms, field of view (FOV) = 220 mm, number of interleaves = 4000, and flip angle = 30°. The 34-ms TR was divided into the following parts: 6 ms for RF, 8 ms for diffusion-encoding, 7 ms for navigation, 8 ms for readout, and 5-ms dead time. The dead time was needed to achieve robust real-time feedback due to constraints particular to our system and not due to any fundamental reason. The scan time was 2 min 16 s per volume. Diffusion gradients were set to 40 mT/m for diffusion-weighted images and to 1 mT/m on all axes for the unweighted image (because setting the diffusion-encoding gradients to 0 would make the sequence a balanced sequence). This resulted in a b-value of approximately 850 s/mm^2 for diffusion-weighted images and 2 s/mm^2 for unweighted images according to calculations based on white matter at 3 T ($T_1 = 1100$ ms, $T_2 = 75$ ms, apparent diffusion coefficient = 0.7×10^{-3} mm^2/s) (17).

The 3D navigator was a stack-of-spirals with seven spiral planes (Fig. 2). Phase-encoding was performed in the z-direction, whereas the spirals lie in the x/y-plane. To save time, even numbered phase-encodes are spiral-in, whereas odd numbered spirals are spiral-out as depicted

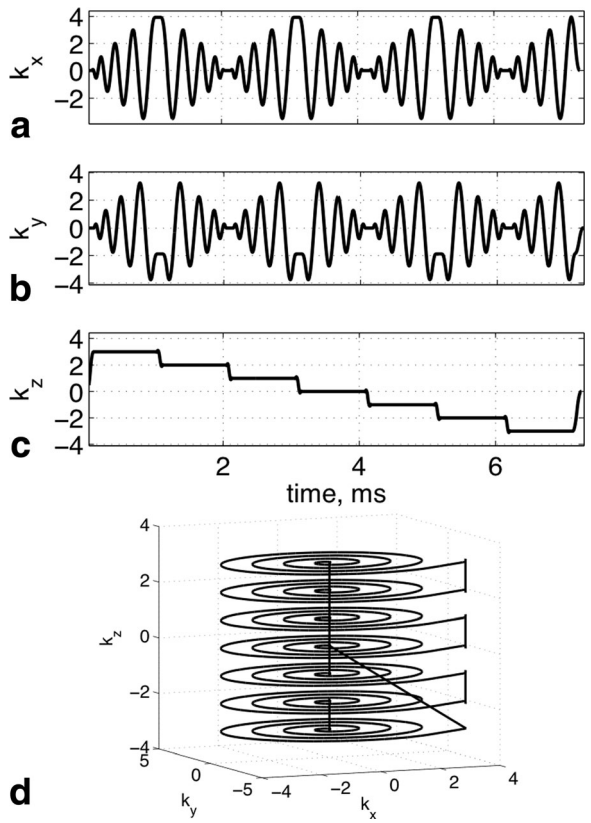

FIG. 2. The waveforms used to generate the 3D navigators as measured on the *x* (**a**), *y* (**b**), and *z* (**c**) axes in units of k-space points and the corresponding trajectory in 3D (**d**).

in Figure 2. The region covered in k-space is a cylinder with a radius of 3 k-space points and a height of 6 k-space points. With the parameters used in this DW-SSFP sequence, a shift of the k-space center of 1 point corresponds to an angular velocity of approximately 1.5 degrees per second about an axis of rotation perpendicular to the diffusion-encoding direction. Therefore, the coverage of the navigator is sufficient to measure angular velocities up to approximately ±4.5 degrees per second.

Prospective correction of RB motion

Prospective correction of RB motion was performed using in-house software run on the manufacturer's built-in real-time processing environment (GE Healthcare, Waukesha, WI). A schematic of the pulse sequence and its interaction with the correction system is provided in Figure 1. Two TRs of the pulse sequence are depicted, since corrections applied in a given TR are collected in the previous TR. Navigator data collected in TR *n* (Fig. 1b) are transferred to the correction routine that is waiting to receive it. Once the routine has received data, navigator images are reconstructed from the raw data by matrix multiplication using a precomputed direct Fourier transform (DFT) matrix.

The DFT-based reconstruction of the navigator image is the most time-consuming step of the real-time processing. To reduce the computation burden, all eight coils were reconstructed only once at the 20th TR of the unweighted scan. In this TR, the coil having the maximum value for each pixel in the reconstructed navigator image is determined. Subsequent images are reconstructed by gridding only the coil with maximum signal magnitude in each pixel. This is achieved in practice by skipping rows of the DFT matrix. After the 20th TR, the navigator images from each TR are summed together to form a high-signal-to-noise ratio (SNR) reference image. At the 100th TR, this reference image is used to form a mask image by thresholding at a level of 30% of the maximum value. This mask image is used to further reduce the computational burden by omitting rows of the DFT matrix that correspond to pixels outside of the region of interest. This mask image and the coil information are then used in all subsequent volumes; they are not recomputed. A final reduction in the computational burden of the DFT multiplication is the reduction in the number of columns by down-sampling along the k-space trajectory. Because the navigator readout is slew limited, it is oversampled along the readout direction. Empirically, it was found that an acceleration factor of four was possible with no detriment to the estimation accuracy of the motion parameters. So, in practice only every fourth point in the navigator data is used in the reconstruction of the navigator image. In total, these reductions bring the DFT reconstruction time down to about 1 ms without any parallel processing.

To avoid any phase effects arising from the transient period at the beginning of each diffusion-weighted volume, the ProCo system begins to send motion estimates after the 100th TR of each volume. The linear phase terms along each axis are computed using the navigator image and the reference image using Eq. [5] (15). Then, the constant phase term is computed by Eq. [6]. These four values (three for linear and one for constant) are then sent to the scanner computer to update the sequence in TR $n+1$. To correct the linear terms, the amplitude of a blip gradient is adjusted to cancel the linear phase dependence measured in TR *n* (Fig. 1d). To correct the constant phase terms, the phase of the RF pulse in TR $n+1$ is set to the value of the previous RF pulse plus the measured constant phase. The receiver phase for the navigator and imaging readouts is set to the same phase as that of the RF pulse (Fig. 1e).

Damping

To reduce instability in the correction system due to noise in the estimation of the motion parameters, a damping parameter was introduced on both the linear and constant phase terms. Damping is needed, not because the estimations of the phase terms are systematically higher, but because any errors in the estimated phase accrue cumulatively into the reference image causing the error to be integrated over time. This results in a random walk of the reference phase that can cause erroneous estimation that then feeds back further error into the system. Damping ensures that the system is always biased toward an equilibrium value and that any fluctuations in the reference value do not propagate. For the linear terms, the damping was achieved by multiplying the calculated correction blip amplitude by 0.8. Effectively, this reduced the requested correction blip by 20%. Similarly, the constant phase term was multiplied by a factor of 0.8. This factor

was chosen empirically based on the level of noise in the navigator data from the diffusion-weighted volumes.

Phantom Validation

To assess the accuracy of the system in determining the induced phase error, the DW-SSFP sequence was used to scan an agar phantom ($T_1 = 900$ ms, $T_2 = 40$ ms). One unweighted image and one diffusion-weighted image (encoding along the S/I direction) were acquired. Motion was simulated by introducing test blips (Fig. 1a) immediately after the diffusion-encoding gradient. The test blips simulate rotational motion on each axis by imposing a known linear phase on the object. The blips were turned on in repeatable pseudorandom order using blips ranging from −1.5 k-space points to 1.5 k-space points on all axes. Four experiments were carried out: (1) no blips without ProCo, (2) blips without ProCo, (3) no blips with ProCo, and (4) blips with ProCo.

Human Subjects

To test the performance of the system on a case of real motion, six healthy human subjects were scanned with the DW-SSFP sequence in a study approved by our institutional review board (#4947). In subjects 1 and 2, four volumes were acquired: one unweighted and three diffusion-weighted volumes with the diffusion-encoding direction along three orthogonal axes—left/right (L/R), anterior/posterior (A/P), and superior/inferior (S/I). In subjects 3, 4, 5, and 6, a DTI protocol consisting of seven isotropically distributed diffusion-weighted volumes and one unweighted volume was acquired. For all subjects, two scans were performed: (1) without ProCo and (2) with ProCo. For subjects 4, 5, and 6, an EPI scan with the same diffusion-encodings was acquired for anatomical reference. Due to a technical error, diffusion-weighted volume six was not acquired in subject 5.

Data Processing

To demonstrate how ProCo affects the signal magnitude for diffusion-encoding along the three cardinal directions, the maximum navigator signal versus TR number was computed by averaging the magnitude of the navigator signal across all coils and taking the maximum value along the readout direction. These signal curves were normalized by the maximum value from all signal curves in all of the diffusion-weighted images acquired in the scans in the human subject.

To compare the data signal magnitude and image signal magnitude from scans with and without ProCo, two comparative metrics were computed for each pair of images acquired with each diffusion-encoding direction, for all subjects. The rationale for examining both signal in the raw data as well as the reconstructed images is to demonstrate the direct effect of ProCo on the steady-state signal magnitude (the raw data) in the absence of post processing as well as on the final product (the images). Because motion causes differential phase change and magnitude loss in k-space, its effect on the images are not obvious, as the signal in a given pixel depends on all of k-space. First, to assess the increase in data signal magnitude observed with ProCo, the percent increase in data signal magnitude, ΔS_D, was computed according to:

$$\Delta S_D = 100 \frac{\overline{|D_{Pro}|} - \overline{|D_{No}|}}{\overline{|D_{Pro}|}}, \quad [8]$$

where D_{Pro} and D_{No} are the data acquired with and without ProCo, respectively, averaged over all k-space readout points and interleaves, for the coil with the maximum signal. Note that, as the receiver gains were not changed between scans, the mean signal is a meaningful measure of relative SNR. Second, to assess the effect of ProCo on the signal magnitude in the reconstructed image, an analogous measure was computed for the image signal magnitude:

$$\Delta S_I = 100 \frac{\overline{|I_{Pro}|} - \overline{|I_{No}|}}{\overline{|I_{Pro}|}}, \quad [9]$$

where I_{Pro} and I_{No} are the images acquired with and without ProCo, respectively. The average here was performed over pixels in a mask. The mask was computed by adding all diffusion-weighted volumes for a given scan together and thresholding at 20% of the maximum signal in the sum of the diffusion-weighted volumes from each subject. Errors in ΔS_D and ΔS_I were estimated by the propagation of errors using the standard deviation of signal at the edge of k-space as an estimate of the error of measurements in k-space and the standard deviation of the signal in a background region of interest as an estimate of the error of measurements in image space.

To assess the regional differences in image signal magnitude of the images with and without ProCo, percent difference maps were calculated. To remove the influence of high-spatial frequency features, the images were first low-pass filtered. Then, the percent difference maps of the low pass filtered images were computed as the magnitude image with ProCo minus the magnitude image without ProCo divided by the magnitude image with ProCo times 100.

For the DTI scan performed in subjects 3, 4, 5, and 6, the fractional anisotropy (FA), principal eigenvector, and color FA were computed from the diffusion tensor. The tensor was computed from the diffusion-weighted images after a spatial filtering step to remove directional bias caused by residual uncorrected motion (8).

EPI Reference

For reference, a 2D diffusion-weighted EPI scan was performed on subjects 4, 5, and 6. Imaging parameters were: 128^2 matrix, 220 mm^2 FOV, echo time (TE) = 80 ms, TR = 4 s, 24 slices, slice thickness 4 mm, slice gap 2.5 mm, b-value = 1000 s/mm^2, and 24 over-scan lines. Ramp-sampled data were gridded to a Cartesian grid and then reconstructed by performing the 2D inverse fast fourier transform (FFT).

Image Reconstruction

Images were reconstructed by gridding to a measured k-space trajectory (18) using precalculated density-compensation weights (19,20). Phantom images were

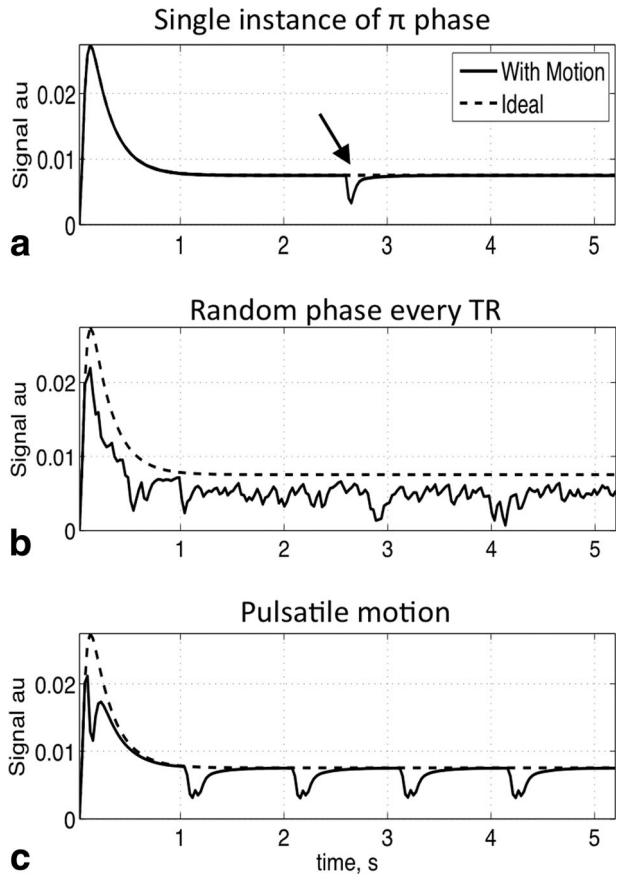

FIG. 3. The steady-state signal in the presence of three types of motion: **(a)** a single motion-induced phase of 180 degrees (arrow), **(b)** random, zero-mean, Gaussian-distributed phase every TR (26 ms), and **(c)** pulsatile motion.

reconstructed with retrospective RB motion correction, whereas the images from the human subjects were reconstructed using retrospective RB and non-RB motion correction (8). Off-resonance correction was performed via block-wise autofocusing (21). Reconstruction and post processing routines were implemented with in-house software developed in MATLAB (Natick, MA) and C++. Gridding and density compensation were implemented using free code from MRI_UNBOUND (http://www.ismrm.org/mri_unbound/sequence.htm).

RESULTS

Simulations

The steady-state signal curves for a single pixel undergoing three distinct types of motions are compared in Figure 3. The effect of a single impulsive motion occurring in only one TR is a sudden drop in signal followed by a transient period of recovery (Fig. 3a, arrow). This transient period is caused by the destructive interference of coherence pathways formed before the motion occurred with coherence pathways formed after the motion occurred that have differing phase. This effect can be thought of as a kind of impulse response of the spin system to motion. Random motion is basically a series of these impulse-type motion events that keep the signal in a constant transient state (Fig. 3b), whereas a periodic pulsatile motion produces periodic drops in signal followed by recovery to steady state (Fig. 3c). This last pattern has been observed in human subjects and is due to the pulsatile cardiac motion (14). Note that, because of the influence of phase errors accrued in one TR on subsequent TR's and the randomness of the phase errors, it is difficult to simply discard and rescan without substantially increasing the scan time.

The size of the "notch" in the steady-state signal (Fig. 3a, arrow) will vary with sequence parameters, flip angle, TR, T_1, T_2, diffusion coefficient, and with the phase induced. In Figure 4, the relative signal loss is plotted versus the phase introduced for several flip angles. This shows that the maximum loss occurs when the transverse phase introduced as a result of motion is 180 degrees, a condition which causes the maximum phase cancellation with future coherence pathways. Also of interest is that when the flip angle increases, the relative amount of signal loss is greater. This is of interest as DW-SSFP allows some flexibility in choosing the flip angle. Note that, in the case of the 180 degrees induced phase and a flip angle of 50 degrees, the worst case shown, the relative signal lost is 900% times TR. This means that the signal loss is equivalent to obtaining 0 signal over nine TRs. Of course, this is spread over a longer time period as indicated by Figure 3a.

Phantom Experiments

Central axial slices from the phantom experiments using the test blips (simulating motion) are compared in Figure 5. The image with no test blips and no ProCo is shown as a reference (Fig. 5a). When test blips are turned on, the image loses intensity due to the loss of phase coherence in the steady state (Fig. 5b). To show that ProCo

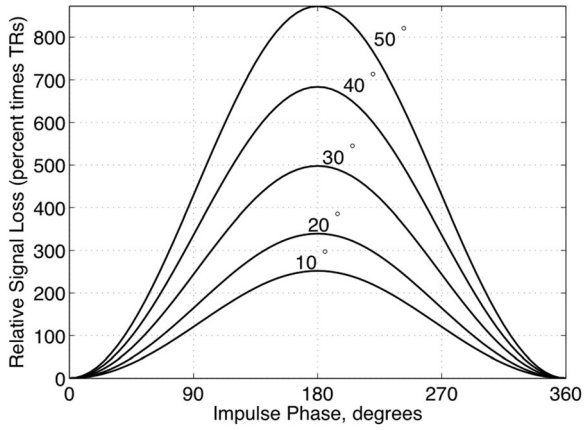

FIG. 4. The relative signal loss due to a motion in a single TR as a function of the phase induced by that motion for flip angles ranging from 10 to 50 degrees (lower curve to upper curve respectively). The signal loss is calculated by integrating the ideal signal minus the motion-corrupted signal over time normalized by the steady-state signal magnitude; essentially this is the size of the "notch" indicated by the arrow in Figure 3a. The greatest loss of signal comes when the induced phase is 180 degrees and increases with flip angle.

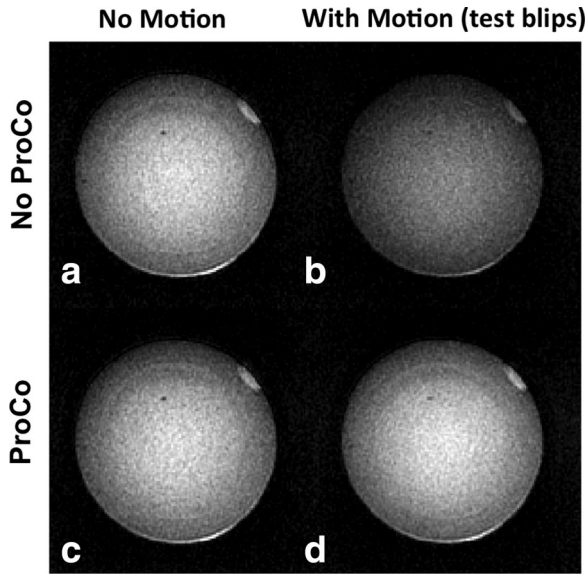

FIG. 5. Central axial slices of a DW-SSFP scan of an agar phantom with simulated linear motion-induced phase errors. The images without motion (**a**,**c**) are compared to images with motion (**b**,**d**) and with (c,d) ProCo. Note that the lower signal observed in the uncorrected case with simulated motion (b) is largely restored with the use of ProCo (d).

does not cause detriment to the image in the absence of motion, the image from a scan without blips with ProCo is shown (Fig. 5c). There is no apparent reduction in the signal magnitude. When the test blips are tuned on with ProCo turned on, the signal magnitude is preserved due to the system's ability to track and correct the phase imposed by the test blips (Fig. 5d). In the image with blips and without ProCo (Fig 5b), the signal magnitude across the whole slice was 70 ± 20, whereas in the other three images (Fig. 5a,c,d) it was 100 ± 20. Note that, in the cases with motion (Fig. 5b,d), there is a slight apparent reduction of spatial resolution compared to the cases without motion (Fig. 5a,c). This is likely due to a change in point spread function caused by the gradient blips used to simulate motion, as each blip shifts k-space trajectory of the interleaf acquired after it. In the case of real motion in vivo, this effect is unavoidable, as motion is involuntary.

Human Subjects

The effect of the ProCo on the signal level in the raw data can be observed in Figure 6. For clarity, only the first 300 TRs of 4000 are shown. In the signal curves from each diffusion-weighted volume from the scan with no ProCo (Fig. 6a), the typical periodic drop in signal magnitude can be observed, with each dip caused by an individual heartbeat. As expected, the most pronounced effects are observed in the S/I-encoded volume (Fig. 6a, green curve). In the scan with ProCo, the same pattern is observed before the correction is activated (Fig. 6b, left of the dashed gray line). When the correction is activated at the 100th TR, the drops in the signals become less pronounced, particularly in the S/I-encoded volume (Fig. 6b, green curve), indicating that ProCo is working.

The percent increases in the data signal magnitude, ΔS_D, and the image signal magnitude, ΔS_I, are given in Table 2. With a few exceptions, all volumes had positive change, indicating that ProCo increased both the raw data signal magnitude and the magnitude in the reconstructed images. The greatest benefit was seen in volumes having diffusion-encoding predominantly along the S/I direction (Table 2, asterisks). The least affected volumes were those with diffusion-encoding predominantly along the A/P direction (Table 2, volumes marked A/P, b and d), likely due to the fact that there is low RB motion along that direction. Note that, the highest values for ΔS_D and ΔS_I were observed in subject 4. This is likely due to that subject moving more than the others.

Although a global assessment of the image signal magnitude with and without ProCo is given in Table 2, the regional variations of the percent difference in signal are depicted in Figure 7 for all subjects and all volumes. The sagittal views are shown as this view best captures the spatial variations in the percent difference. In agreement with Table 2, ProCo has higher signal in the majority of volumes (Fig. 7, warm colors). However, there were regions in four out of the 33 volumes acquired in which ProCo had lower signal (Fig. 7, cool colors, white arrows). In these regions, the greatest difference was on the order of -5% and occurred in the A/P volume or in volume D (encoding vector $[0.6,-0.8,0]$). This may be due to a low component of RB motion in the A/P direction and hence ProCo fitting regional components of non-RB motion. Note, however, that in all volumes, there are regions where ProCo increased the signal magnitude compared to the case without ProCo.

A summary of images acquired in subject 4 are presented in Figure 8. Central axial slices from the scans

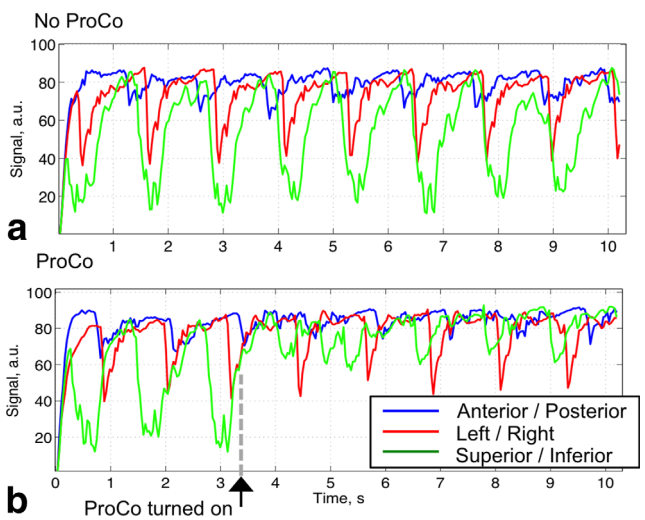

FIG. 6. The maximum value in the raw navigator signal is plotted for the first 300 TRs of each diffusion-weighted volume acquired in the healthy human subject. The A/P (blue lines), L/R (red lines), and S/I (green lines) volumes are plotted together for the scan with no ProCo (**a**) and the scan with ProCo (**b**). Note that the large periodic drops (due to cardiac pulsation) in the signal in the volume with S/I encoding (green line, a) are largely reduced in the scan with ProCo (green lines, b) once ProCo is turned on at TR number 100 (after the dashed gray line, b). [Color figure can be viewed in the online issue, which is available at wileyonlinelibrary.com.]

Table 2
Percent Increase in Data Signal Magnitude (ΔS_D) and Image Signal Magnitude (ΔS_I) with ProCo for All Human Subjects for All Diffusion-Weighted Volumes Acquired; Errors are in Parentheses.

	Subject	L/R	A/P	S/I*				
Three-direction scans: diffusion-encoding volume								
ΔS_D	1	6(10)	8(10)	26(10)				
	2	5(10)	6(11)	22(13)				
ΔS_I	1	8(6)	1(6)	15(7)				
	2	9(8)	0(8)	24(9)				
	Subject	*a*	*b*	*c**	*d*	*e**	*f**	*g**
Seven-direction scans: diffusion-encoding volume								
ΔS_D	3	5(9)	3(8)	24(9)	8(8)	22(9)	17(9)	3(10)
	4	24(9)	19(9)	42(10)	19(9)	33(12)	35(10)	41(10)
	5	3(8)	7(8)	21(9)	6(8)	17(9)	–	14(9)
	6	6(7)	9(8)	30(9)	12(8)	30(10)	28(9)	18(10)
ΔS_I	3	14(8)	2(8)	16(8)	−2(8)	19(8)	17(8)	2(8)
	4	14(7)	6(7)	38(8)	10(7)	29(9)	34(8)	40(8)
	5	14(6)	3(7)	19(7)	0(7)	18(8)	–	9(7)
	6	14(6)	3(6)	27(7)	4(7)	30(8)	23(8)	20(7)

Positive numbers indicate that ProCo had higher signal. Diffusion-encoding directions for each volume are as follows: a:(1,0,0), b:(0.3,0.9,0), c:(−0.3,0.5,0.8), d: (0.6,−0.8,0), e: (0.3,−0.5,0.8), f:(−0.6,0.4,0.7), g:(0.6,0.4,0.7), in which (1,0,0) is L/R, (0,0,1) is A/P, and (0,0,1) is S/I. Volumes in which the absolute value of the S/I component is greater than or equal to 0.7 are marked with an asterisk (*). Note that, in general, the greatest increases are observed when the diffusion-encoding vector points predominantly along the S/I direction (volumes marked with *).

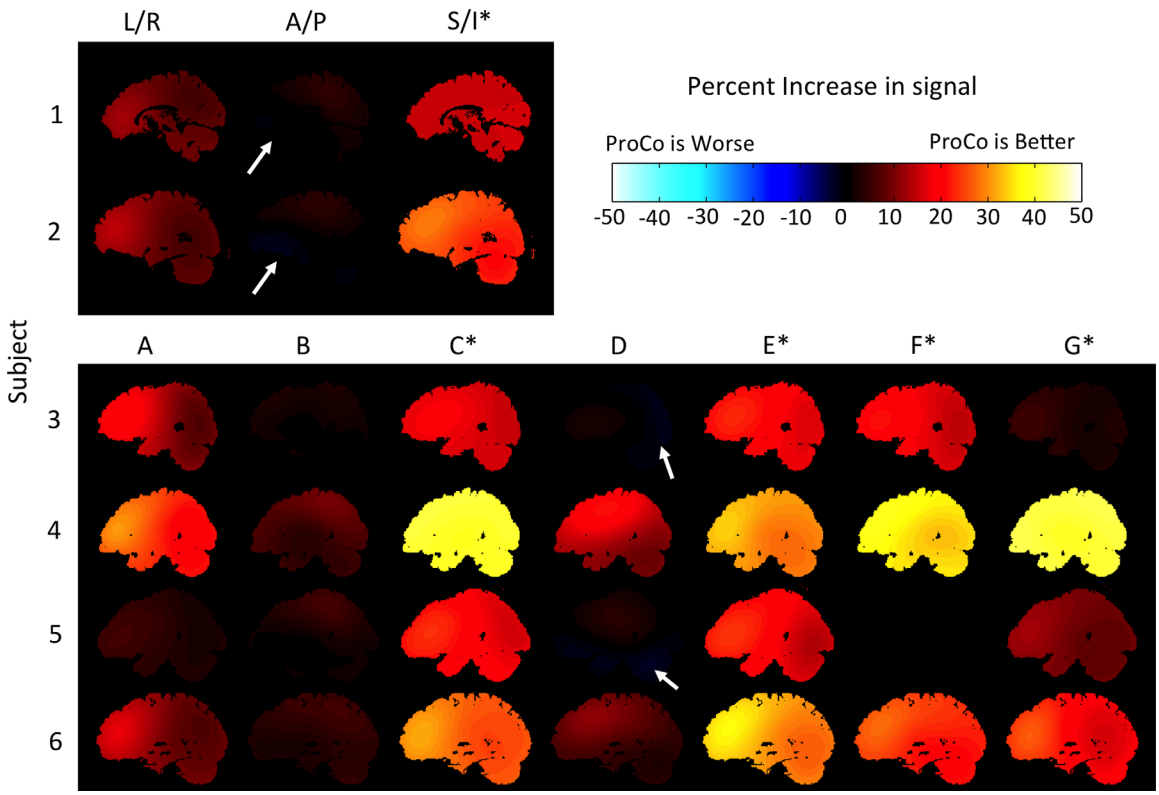

FIG. 7. Sagittal views of the percent difference of image signal magnitude with ProCo and without ProCo for all volumes and all subjects. Areas in which the magnitude with ProCo was higher appear in warm colors, whereas areas in which the signal was lower appear in the cool colors and are marked with white arrows. Only four volumes had areas in which ProCo was worse. Diffusion-encoding directions for each volume are as follows: (**a**) (1,0,0), (**b**) (0.3,0.9,0), (**c**) (−0.3,0.5,0.8), (**d**) (0.6,−0.8,0), (**e**) (0.3,−0.5,0.8), (**f**) (−0.6,0.4,0.7), (**g**) (0.6,0.4,0.7), in which (1,0,0) is L/R, (0,0,1) is A/P, and (0,0,1) is S/I. Volumes in which the absolute value of the S/I component is greater than or equal to 0.7 are marked with an asterisk (*). [Color figure can be viewed in the online issue, which is available at wileyonlinelibrary.com.]

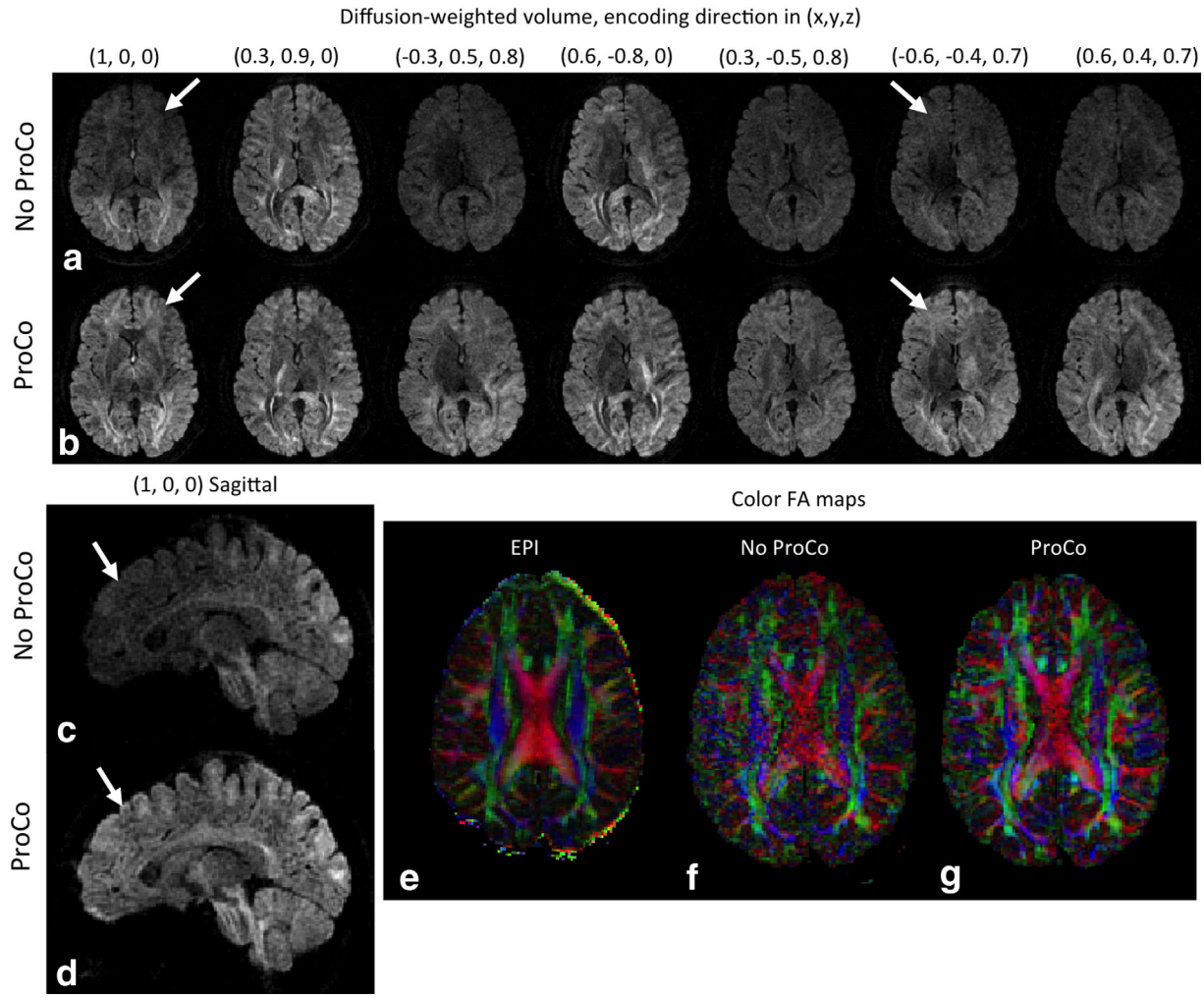

FIG. 8. A comparison of images with and without ProCo from subject 4. In general, the images with ProCo have higher signal magnitude than those acquired without ProCo and in particular there are several regions where this effect is more noticeable (**a–f**, white arrows). This increase in signal with ProCo, particularly in the images with diffusion-encoding directions near the S/I direction, manifests itself in the color FA maps as more accurate representation of white matter tracts running along the S/I direction, such as the posterior limb of the internal capsule (**g**,**h**, white arrows). [Color figure can be viewed in the online issue, which is available at wileyonlinelibrary.com.]

without ProCo (Fig. 8a) are compared to those with ProCo (Fig. 8b) for all seven volumes, demonstrating that the images acquired with ProCo are comparable in quality to those without ProCo across all seven diffusion-weighted volumes. Furthermore, the signal level in certain volumes is higher in the scan with ProCo than the same volume without ProCo (Fig. 8a,b, white arrows). Sagittal (Fig. 8c,d) reformats of the first volume acquired with and without ProCo are compared, showing the increased signal level of the image with ProCo compared to the image without (Fig. 8c,d white arrows). A color FA map from a slice of the EPI image (Fig. 8e) is compared to analogous axial reformats of the color FA maps from the DW-SSFP scans with and without ProCo (Fig. 8f,g). Although both maps depict the white matter tracts appearing in the EPI reference scan, the color FA map from the scan with ProCo (Fig. 8g) has apparently higher SNR than the scan without ProCo (Fig. 8f). Note that, the EPI scan had thicker slices and bigger voxels and therefore appears less noisy than the DW-SSFP scans.

DISCUSSION

The results of this study indicate that, in the presence of motion, the use of prospective correction of RB motion-induced phase can result in higher signal magnitudes in the raw data acquired with DW-SSFP sequences and that these increases in raw signal magnitude lead to increases in the signal magnitude of the resulting images. In particular, for the phantom scans, in which there was purely RB motion by design, the signal magnitude values in the images with motion acquired with ProCo were nearly indistinguishable from those in the images in the absence of motion. In the scans of human subjects, in which motion was composed of both RB and non-RB motion, the signal magnitudes (both of data and images) observed with ProCo were higher in general than those without ProCo. In particular, the greatest benefits with ProCo were observed in the volumes with diffusion-encoding directions along or near the S/I direction. These results are encouraging and indicate that the

system may be used to address the main obstacle to the use of DW-SSFP.

In principle, the proposed ProCo is similar to those that have been proposed and demonstrated for RARE (9) and FLASH (10); however, there are some differences. First, the ProCo system in this work was implemented on unmodified hardware on a clinical MRI system, making it somewhat challenging to achieve the rapid turnaround-time needed in DW-SSFP (<10 ms). This work demonstrates that with the acceleration methods proposed herein, this rapid turnaround time is not a limitation on a clinical MRI system. A second difference between the proposed method and previous work is that the proposed method includes a sliding window reference image to compensate for drift in the B_0, shim and eddy currents.

In this study, the best results were achieved using a combination of retrospective correction and ProCo. This should not be interpreted as evidence of inaccuracies of the prospective correction. Retrospective corrections served two purposes in this study. The first and most obvious is that they were used to correct the non-RB motion in the human case as ProCo was only meant for RB errors. The second use of the retrospective correction was to correct the RB motion-induced shot-to-shot phase inconsistencies that were not corrected by ProCo due to the application of the ProCo correction after the acquisition of the imaging readout. In principle, this second use of retrospective corrections could be eliminated if the total time for ProCo could be reduced to less than 1 ms, allowing the application of the ProCo corrections before the imaging readout; however, this is currently infeasible due to hardware limitations.

A well-known difference of DW-SSFP from spin-echo-based diffusion-weighted methods is the dependence of the diffusion attenuation on sequence parameters such as flip angle and diffusion-encoding gradient duration as well as physical parameters such as T_1, T_2, and diffusion coefficient. In this study, the approximation of Wu and Buxton (17) was used to estimate the *b*-value of the sequence to provide an approximate value for comparison to a spin-echo-based reference method. Although an exact solution exists (22), it would still only be approximate for the whole volume due to the aforementioned dependencies. For the approach taken here, this is not of great concern, as the aim here is to obtain the direction of the white matter fibers in a particular voxel rather than an accurate measure of the apparent diffusion coefficient. An alternative application for the techniques developed in this work that would require a qualitatively accurate solution to the signal equation is the imaging of cartilage in the knee similar to recent work by Staroswiecki et al. (23). In this work, the dual-echo version of DW-SSFP is used to solve the signal equation for T_2 and apparent diffusion coefficient. ProCo as presented here would be well-suited for the knee as motion in the knee tends to be RB motion and largely lacks the pulsatile cardiac component that is present in the brain.

The ProCo methodology proposed in this work is a first step toward addressing the phase-sensitivity of DW-SSFP. Although improvements in the signal magnitude of all diffusion-weighted images were observed with the use of ProCo, there were still residual periodic signal drops in the human case. It is hypothesized that these residual drops in signal were due to non-RB motion-induced phase errors. Because these errors have supralinear spatial dependence, an approach based on tailored RF pulses similar to that proposed by Nunes et al. (11) is needed. This presents a challenge from the standpoint of RF design and may require the use of parallel transmit to achieve the desired phase profiles in 3D. Recently, it has been shown that reasonable 3D phase profiles can be achieved with RF pulses of around 8 ms in duration without recourse to parallel transmit (24). With a suitable prescan to measure phase profiles in the subject, it may be possible to design a set of RF pulses to prospectively correct the non-RB part of the phase. Such an approach would be compatible with the ProCo method presented here, and would address all of the sources of motion-induced phase errors for DW-SSFP. This is the subject of a forthcoming study that is currently underway.

CONCLUSIONS

In this work a novel, prospective correction of motion-induced phase for DW-SSFP was proposed. The correction was implemented on a clinical MRI system and was demonstrated to be feasible in scans of an agar phantom with simulated motion and in human subjects. In nearly all cases, the images with prospective motion correction had higher signal levels than those without correction. In the phantom case, the signal levels in the images with prospective motion correction were nearly the same as those without motion. In the images acquired in human subjects, the signal magnitude in all volumes were higher with ProCo than without. Notable increases in the signal magnitude and diffusion contrast in the volume with S/I-encoding were observed in the images acquired with ProCo compared to those without. In the future, this system could help mitigate the sensitivity of DW-SSFP sequences to motion-induced phase, and enable their use in clinical assessment of white matter integrity.

ACKNOWLEDGMENTS

The authors gratefully acknowledge research support from GE healthcare, especially support on the real time processing systems from Dan Rettmann and Ajit Shankaranarayanan. The authors also acknowledge their funding sources.

REFERENCES

1. Ordidge R, Helpern J, Qing Z, Knight R, Nagesh V. Correction of motional artifacts in diffusion-weighted MR images using navigator echoes. Magn Reson Imag 1994;12:455–460.
2. DeCrespigny A, Marks M, Enzmann D, Moseley M. Navigated diffusion imaging of normal and ischemic human brain. Magn Reson Med 1995;33:720–728.
3. Butts K, de Crespigny A, Pauly J, Moseley M. Diffusion-weighted interleaved echo-planar imaging with a pair of orthogonal navigator echoes. Magn Reson Med 1996;35:763–770.
4. Skare S, Newbould RD, Clayton DB, Bammer R. Propeller EPI in the other direction. Magn Reson Med 2006;55:1298–1307.

5. Miller KL, Hargreaves BA, Gold GE, Pauly JM. Steady-state diffusion-weighted imaging of in vivo knee cartilage. Magn Reson Med 2004; 51:394–398.
6. Jung Y, Samsonov A, Block W, Lazar M, Lu A, Liu J, Alexander A. 3D diffusion tensor MRI with isotropic resolution using a steady-state radial acquisition. J Magn Reson Imag 2009;29:1175–1184.
7. McNab J, Gallichan D, Miller K. 3D steady-state diffusion-weighted imaging with trajectory using radially batched internal navigator echoes (TURBINE). Magn Reson Med 2010;63:235–242.
8. O'Halloran R, Aksoy M, Van A, Bammer R. 3D isotropic high-resolution diffusion-weighted MRI of the whole brain with a motion-corrected steady-state free precession sequence. Magn Reson Med 2013;70:466–478.
9. Norris DG, Driesel W. Online motion correction for diffusion-weighted imaging using navigator echoes: Application to RARE imaging without sensitivity loss. Magn Reson Med 2001;45:729–733.
10. Weih K, Driesel W, von Mengershausen M, Norris D. Online motion correction for diffusion-weighted segmented-EPI and FLASH imaging. Magn Reson Mater Phys Biol Med 2004;16:277–283.
11. Nunes RG, Malik SJ, Hajnal JV. Single shot fast spin echo diffusion imaging with correction for non-linear phase errors using tailored RF pulses. Magn Reson Med 2014;71:691–701.
12. O'Halloran R, Holdsworth S, Aksoy M, Bammer R. A model for the correction of motion-induced phase errors in multi-shot dw-mri of the head: Are cardiac-motion-induced phase errors reproducible from beat to beat? Magn Reson Med 2012;68:430–440.
13. Anderson A, Gore J. Analysis and correction of motion artifacts in diffusion weighted imaging. Magn Reson Med 1994;32:379–387.
14. Gudbjartsson H, Patz S. Simultaneous calculation of flow and diffusion sensitivity in steady-state free precession imaging. Magn Reson Med 1995;34:567–579.
15. Ahn C, Cho Z. A new phase correction method in NMR imaging based on autocorrelation and histogram analysis. IEEE Trans Med Imag 1987;6:32–36.
16. Irarrazabal P, Nishimura D. Fast three dimensional magnetic resonance imaging. Magn Reson Med 1995;33:656–662.
17. Wu E, Buxton R. Effect of diffusion on the steady-state magnetization with pulsed field gradients. J Magn Reson 1990;90:243–253.
18. Duyn J, Yang Y, Frank J, van der Veen J. Simple correction method for k-space trajectory deviations in MRI. J Magn Reson 1998;132:150–153.
19. Pipe J, Menon P. Sampling density compensation in MRI: rationale and an iterative numerical solution. Magn Reson Med 1999;41:179–186.
20. Johnson K, Pipe J. Convolution kernel design and efficient algorithm for sampling density correction. Magn Reson Med 2009;61:439–447.
21. Smith TB, Nayak KS. Automatic off-resonance correction in spiral imaging with piecewise linear autofocus. Magn Reson Med 2013;69: 82–90.
22. Freed D, Scheven U, Zielinski L, Sen P, Hürlimann M. Steady-state free precession experiments and exact treatment of diffusion in a uniform gradient. J Chem Phys 2001;115:4249.
23. Staroswiecki E, Granlund KL, Alley MT, Gold GE, Hargreaves BA. Simultaneous estimation of T2 and apparent diffusion coefficient in human articular cartilage in vivo with a modified three-dimensional double echo steady state (DESS) sequence at 3T. Magn Reson Med 2012;67:1086–1096.
24. Aboussouan E, Van A, O'Halloran R, Holdsworth S, Alley M, Aksoy M, Bammer R. Estimation and compensation of motion-induced phase error in 3D for multi-shot diffusion acquisitions. In Proceedings of the 21st Annual Meeting of ISMRM, Salt Lake City, Utah, USA, 2013. Abstract 2084.